



# F61 Nuclear magnetic resonance

## Long Report

Nils Schmitt      Timo Kleinbek

Conducted in August 2018  
Supervisor: Minjung, Kim

### Abstract

*In this experiment we started by studying the basics of magnetic excitation. In particular, we wanted to understand how exactly nuclear spins are excited to perform Larmor precession. We measured the relaxation time in the first part of the experiment. In the second part, we identified different substances by comparing the measured shifts of the Larmor frequency caused by different molecular structures. Lastly, we used nuclear magnetic resonance and different imaging methods to take pictures of several objects, analogously to the medical MRI treatment.*

## Contents

1. Theoretical Basics	1
2. Measurements Log and Evaluation	8
3. Critical Comment	14

## 1. Theoretical Basics

### Basics and the relaxation time

In an applied external magnetic field, existing magnetic moments of the atomic nuclei in a material align themselves along the external magnetic field, parallel or anti-parallel. The corresponding energy splitting is given by the scalar product of magnetic moment and external magnetic field in the form

$$\Delta E = -\mu \cdot B_0. \quad (1)$$

The parallel alignment is energetically lower.

The proton population numbers correctly described by the Fermi-Dirac statistics can be approximated classically by the Boltzmann distribution. The ratio of the two occupation numbers with parallel and antiparallel alignment is then given by

$$\frac{N_+}{N_-} = e^{\frac{2\Delta E}{k_B T}}. \quad (2)$$

An estimate in which the magnetic moment is approximately one Bohr's magneton and the magnetic field is approximately 1 T results in a difference between the two occupation numbers of approximately one per thousand at room temperature.

The total magnetization results from the sum of these thousandth part over the whole substance. In general, the following applies from the electrodynamics for the resulting torque from a magnetic field and a magnetization

$$\tau = M \times B_0. \quad (3)$$

For (anti-)parallel alignment, the torque is zero. As soon as  $B_0$  and  $M$  span a plane, the resulting torque rotates the magnetization around the axis of the magnetic field with the Larmor frequency

$$\omega_L = \gamma B_0. \quad (4)$$

Now we create a second magnetic field  $B_1$  orthogonal to a relatively strong external magnetic field  $B_0$ . Before the magnetization can align itself along the new total magnetic field  $B_{\text{tot}}$ , the Larmor precession around this begins. If the magnetic field  $B_1$  oscillates with the Larmor frequency of the atomic nuclei, the magnetization can be deflected, as schematically shown in figure 1. With the

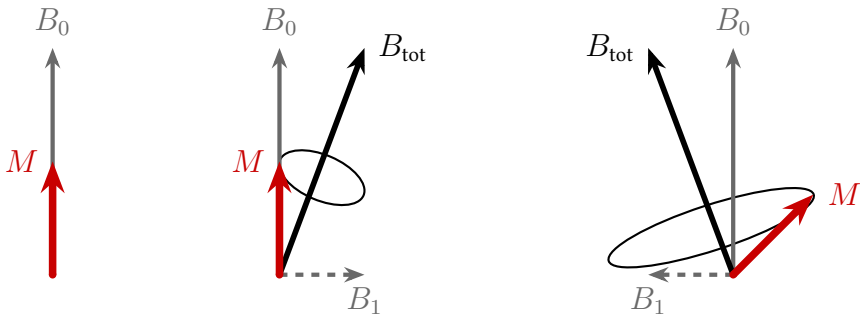


Figure 1: High-frequency external magnetic field generates elongation of magnetization.

duration of the applied high-frequency magnetic field  $B_1$  we can determine the angle by which the magnetization is deflected compared to the external magnetic field  $B_0$ . In particular, so-called 90° and 180° pulses can be generated, which generate an orthogonal or antiparallel magnetisation to  $B_0$  from a parallel magnetisation.

For these excited states of magnetization, the Bloch equations result in an asymptotic drop on characteristic time scales for antiparallel and orthogonal magnetization respectively  $T_1$  and  $T_2$ :

$$M_{||}(t) = M_0 \cdot \left(1 - 2e^{-\frac{t}{T_1}}\right) \quad (5)$$

$$M_{\perp}(t) = M_0 \cdot e^{-\frac{t}{T_2}} \quad (6)$$

The decay of the anti-parallel magnetization is caused by the interaction of the spins with the external magnetic field  $B_0$  (spin-lattice changer effect), whereas interactions between the individual spins (spin-spin interaction) lead to the decay of the parallel magnetization. Since the spin-spin interaction is stronger than the spin-lattice interaction,  $T_2 \leq T_1$  is expected.

Measurements of orthogonal magnetization are made in the  $B_1$  generating coil by induction. After switching off the  $B_1$  field, the precession of the magnetization around the external magnetic field  $B_0$  induces an alternating current in the  $B_1$  coil. This can be measured on a connected oscilloscope. In our setup, the output signal of the induction coil leads back again into the signal generator, which generates the high-frequency alternating field  $B_1$ , and only then into the readout devices. Thus we see the final signal as a superposition of the signal frequency and the alarm frequency, which shows the sum and difference of the two frequencies. We also call the difference the operating frequency, which is a few hundred hertz; this difference is in the per thousand range relative to the larmor frequency of hydrogen nuclei (about 20 MHz).

The relaxation time  $T_1$  can be measured by first passing a  $180^\circ$  pulse an antiparallel orientation of the magnetization is caused and then after different time intervals a  $90^\circ$  pulse generates a signal in the induction coil whose amplitude is proportional to the magnitude of the antiparallel magnetization of before the  $90^\circ$  pulse. By recording these amplitudes after different times, the exponential decrease of the antiparallel magnetization can be investigated and  $T_1$  determined.

The relaxation time  $T_2$  is measured by another combination of  $90^\circ$  and  $180^\circ$  pulses. First a  $90^\circ$  pulse produces a magnetization perpendicular to the  $B_0$  field, which because of this field begins to precessionize this axis with the Larmor frequency. However, the external magnetic field is designed so that the magnetic field strength varies in the direction of the magnetic field vector. Because the Larmor frequency by equation 4 dependence at the different coordinates. This incoherence reduces the amplitude of the induced field in the coil. After a certain period of time  $\tau$  a  $180^\circ$  pulse is sent, which causes a mirroring around  $180^\circ$  on an axis perpendicular to the axis of the  $B_0$  field around which the magnetization rotates. The consequence of this mirroring is that the nuclei that were previously in phase after the other nuclei are now at the same phase angle in front of them. The previous phase difference was due to the precession during a time  $\tau$  had arisen. By mirroring through the  $180^\circ$  pulse, after a further precession period of  $\tau$ , the nuclei are all in phase again and thus show a maximum induction current. This allows the magnitude decrease to be measured over a period of  $2\tau$ .

Now you can always use different values for  $\tau$  and measure the decrease of the amplitude after twice the time to reconstruct the exponential decrease and so  $T_2$ . This measuring method is called spin-echo method.

Alternatively, another  $180^\circ$  pulse can be sent to all odd multiples of time  $\tau$  so that a maximum induction current is measured at all even multiples of  $\tau$  and the relaxation time can be determined from this. This sequence of one  $90^\circ$  and several  $180^\circ$  pulses is called the Carr-Purcell sequence. The basic procedure of the process described here is shown in figure 2 is illustrated.

## Chemical Shift

When considering the excitation of nuclear spins, only atoms that actually have a nuclear spin can be excited (i. e.  $S \neq 0$ ). Of course, a single proton as fermion in the nucleus of a hydrogen atom has

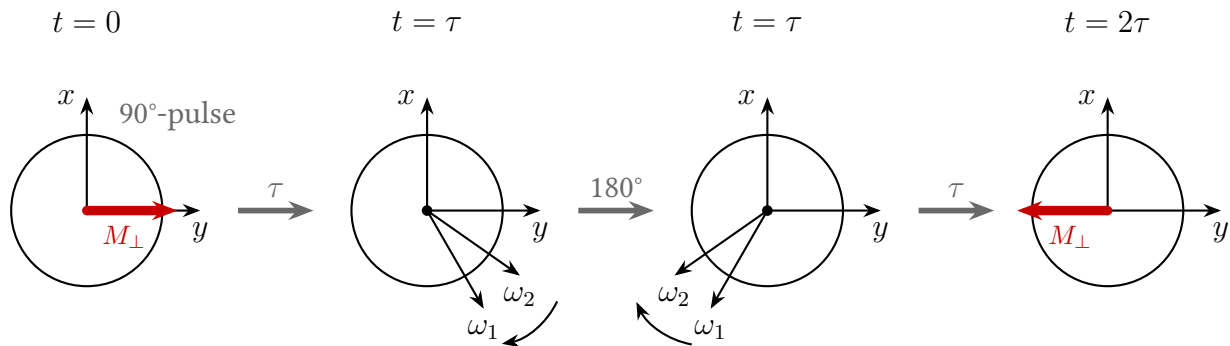


Figure 2: Diagram for measuring the relaxation time  $T_2$ .

a spin of  $S = 1/2$ . On the other hand, for a carbon atom, for example  $S = 0$ , so there is no magnetic moment at all that could contribute to magnetization.

Additionally, note that the  $90^\circ$  and  $180^\circ$  pulses are always adjusted to a noise frequency. In order to achieve an effective excitation of nuclear spins of different atoms, the gyromagnetic ratio must also be the same. If we expose a sample of organic material to only one frequency that excites hydrogen nuclei, only the hydrogen atoms of an organic material will contribute to the measured larmor frequency. In different molecules the hydrogen molecules are present in different bonds with different electronegativity differences, which means that the probability of residence of the electrons around the proton is not always the same. Due to this difference, the externally applied magnetic field  $B_0$  is also shielded to different degrees by the electron, which results in a slightly different larmor frequency. The shielded part of the magnetic field is described by

$$\delta \mathbf{B} = -\sigma \mathbf{B}_0, \quad (7)$$

where  $\sigma$  is the proportionality factor. For a certain material, the changed Larmor frequency results accordingly from the superposition of both magnetic fields to

$$\omega_i = \omega_L(1 - \sigma_i). \quad (8)$$

In order to identify a sample on the basis of this shift of the Larmor frequency, the shielding factors relative to a reference sample (here Tetra-Methyl-Silane, short TMS) are measured by measuring the distance of the corresponding resonance peaks. This distance then corresponds to

$$\delta_i \cdot \omega_L = \omega_{\text{TMS}} - \omega_i. \quad (9)$$

The differences of the shielding factors  $\delta_i = \sigma_i - \sigma_{\text{TMS}}$  can then be looked up in a table as shown in figure 3.

The positions of the molecules in this list can be explained using the example of a COOH group. Here, the hydrogen atom is directly bonded to an oxygen atom with a relatively high electronegativity, while a second oxygen atom is bonded directly to an oxygen atom with a relatively high electronegativity. oxygen atom is still in the immediate vicinity. The hydrogen atom itself is thus virtually “naked” and is hardly shielded from its electron, which leads to a stronger effective magnetic field compared to C-H bonds and thus to an increased larmor frequency.

## Imaging Techniques

By excitation of nuclear spins and subsequent measurement of the magnetization, the distribution of the excited spins can be reconstructed under certain conditions and thus one-, two- or three-dimensional images of the nuclear spin distribution can be generated. To divide the material into

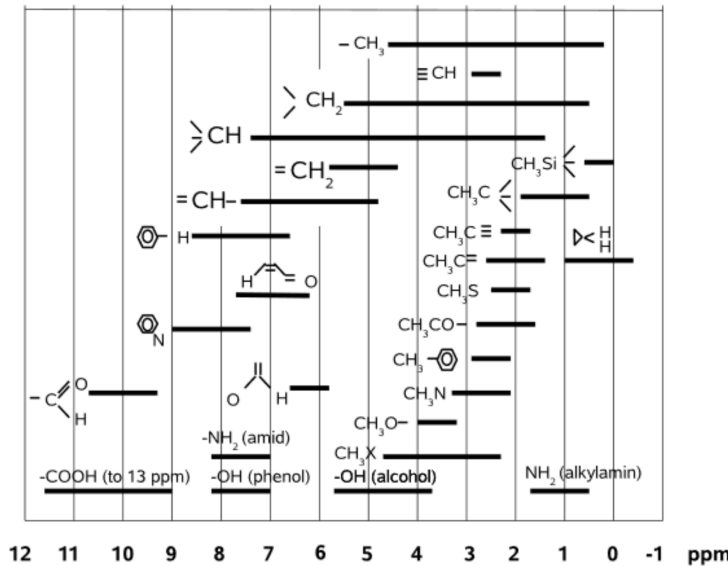


Figure 3: Chemical shifts of different molecules relative to TMS [1].

readable pixels in the different dimensions, in addition to an external  $B_0$  field along the direction, which we now define as  $z$  direction, we use magnetic fields, which also point in  $z$  direction but change spatially with the  $x$ ,  $y$  or  $z$  coordinate. In  $x$  direction, for example:

$$\mathbf{B}_x = (0, 0, G_x x)$$

### Frequency Coding

After equation 4 the Larmor frequency in a magnetic field, which is superimposed by  $B_0$  and a field varying in  $z$  direction, results to

$$\omega_L(z) = \gamma(B_0 + G_z z) = \omega_L^0 + \omega_z. \quad (10)$$

As soon as a  $90^\circ$  pulse causes a magnetization in the  $x - y$  plane, this precedes the  $z$  position with different alarm frequency around the axis of the magnetic field. The signal generated in an adjacent induction coil whose axis must be perpendicular to the  $z$  direction is then proportional to the sum of all magnetizations multiplied by the phase resulting from the high frequency of the  $90^\circ$  pulse

$$S(t) \sim \int_V M_{\perp}(z, t) e^{-i\omega_{HF}t} dV \quad (11)$$

what is equal to

$$S(t) \sim \int_V M_{\perp}^{\text{rot}}(z, t) e^{-i(\omega_L^0 + \omega_z - \omega_{HF})t} dV. \quad (12)$$

If we assume that  $\Omega = \omega_L^0 - \omega_{HF}$ , the exponential function before the integral only contributes a phase and we get

$$S(t) \sim e^{i\Omega t} \int_Z \left( \int_X \int_Y M_{\perp}^{\text{rot}}(z, t) dy dx \right) e^{i\omega_z t} dz. \quad (13)$$

After integration over the area of the induction coil, the measured signal is thus proportional to the Fourier transform of the magnetization. By measuring the signal at different times  $t_i$  the distribution of the magnetization depending on the position  $z$  can be calculated by discrete Fourier transformation. As usual for functions that are linked via Fourier transform, the product of characteristic widths of the functions is constant.

Therefore, the following applies

$$\Delta z \sim \frac{1}{\Delta t}. \quad (14)$$

The nuclear spins along the  $z$  coordinate have because of the inhomogeneous magnetic field different Larmor frequencies and the information of the position is “encoded” by these frequencies. Therefore we also call this method frequency coding.

For the resolution of a two-dimensional image we cannot simply use a apply inhomogeneous magnetic field in an additional direction because the two fields would superimpose each other and the magnetization would occur along the corresponding diagonals. Rather, we need a second type of coding, which we find in phase coding.

## Phase Coding

By applying an inhomogeneous magnetic field and the different Larmor frequency, a phase difference

$$\Delta\phi(z) = \phi(z) - \phi(0) = \gamma G^z z t = \omega_z t \quad (15)$$

between the nuclear spin. If we create such a field for a fixed time  $T_{\text{Ph}}$ , the phase is dependent on the  $z$ -coordinate in the form

$$\phi(z) = \gamma G^z T_{\text{Ph}} z = k_z z. \quad (16)$$

Similar to the steps above, signal and magnetization are again linked via Fourier transformation. Instead of creating several measuring points over time, different in the phase coding, the  $k_z$  implicitly defined above is obtained by varying the magnetic field gradient or the action time and thus receive a collection of measuring points that can be transformed back.

## Two dimensional imaging

As already mentioned, we now use both of the coding possibilities mentioned to create two-dimensional images. For a three-dimensional sample, we must first select a thin layer from which we want to generate the two-dimensional image. This selection is made by selective excitation of the nuclear spins in the layer to be examined. In a magnetic field gradient, for a layer whose  $z$  coordinate is between  $z_1$  and  $z_2$ , the Larmor frequencies are also between corresponding frequencies  $\omega_1$  and  $\omega_2$ . The transmission of a square-wave signal in the frequency space between these frequencies allows selective excitation of the desired layer.

Then the nuclear spins can be encoded one after the other in the two dimensions as illustrated in figure 4. In a first step, by applying an inhomogeneous magnetic field in  $x$  direction, different phases can be assigned to the spins in  $x$  direction, which are retained after switching off the additional inhomogeneous field, because then all spins again further precise with the same alarm frequency. In the last step, an inhomogeneous field is created in the  $y$  direction and the  $y$  direction is encoded in

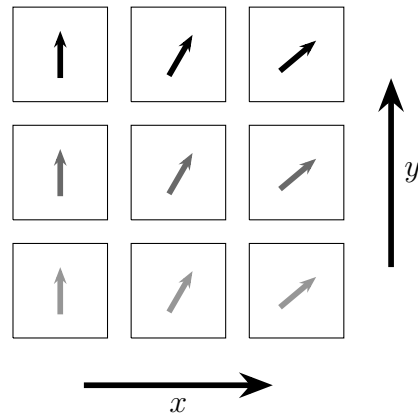


Figure 4: Spins for two-dimensional images, where the direction of the arrow symbolizes the phase and the grayscale the frequency.

different frequencies. Here a data set is recorded directly in a certain time interval. To scroll through the pixels in the  $x$  direction, the  $k_z$  must be changed again. This produces a two-dimensional data set, which is again transformed into an image by two-dimensional inverse Fourier transformation. of the magnetization can be translated. The procedure of this data acquisition is shown in figure 5. It is obvious that by stimulating individual layers and creating the respective images one after the

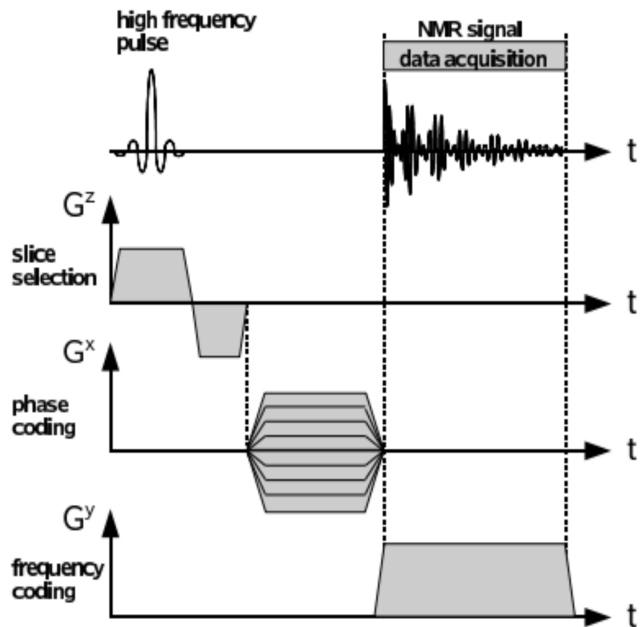


Figure 5: Data recording for two-dimensional imaging [1].

other, three-dimensional objects can also be examined.

## 2. Measurements Log and Evaluation

### Experimental setup

The relaxation times and the chemical shift were measured with a Bruker minispec p20 (see fig. 6). The arrangement is divided into the p20 electrical unit and the p20 magnet.

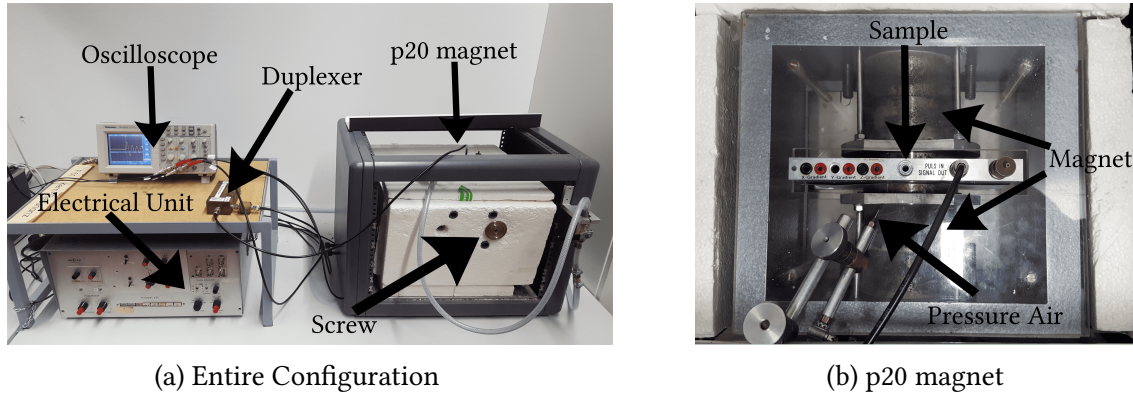


Figure 6: Experimental setup.

The electrical unit can generate two different pulses (hereinafter called pulse I and pulse II), as well as I-I, I-II and II-I sequences and a Carr-Purcell sequence. For the sequences the duration between the individual pulses and for the individual pulses the pulse duration can be set. The latter was later adjusted so that the two pulses correspond to a  $90^\circ$  or  $180^\circ$  pulse. The signal generated by the electrical unit is conducted into the magnet, where it generates a magnetic field that deflects the magnetic moments of the atomic nuclei in the sample. These rotate as described in the previous section now with the Larmor frequency and generates a signal with this frequency in an induction coil inside the structure, which is fed back into the electronic unit via the duplexer, where it is modulated with the high-frequency excitation frequency. The resulting signal has an operating frequency which indicates the difference between the excitation frequency and the Larmor frequency. This is displayed on the oscilloscope and read out and evaluated on the PC with LabView.

### Determination of relaxation time

#### Spin-spin interaction $T_2$ using spin-echo method

As described in the theoretical principles, different time spans  $\tau$  were set as the interval duration between the  $90^\circ$  pulse and the  $180^\circ$  pulse and the intensity of the observed echo was measured after each period of  $2\tau$ , when all spins again contributed in phase to a maximum induction current.

When measuring the Gd500 sample we regularly checked the working frequency values and found that this value increased from initially  $\omega_f = (900 \pm 40)$  Hz to now  $\omega_f = (1150 \pm 20)$  Hz and finally to  $\omega_f = (1170 \pm 20)$  Hz. The reason for this is a change in the alarm frequency of the hydrogen atoms due to a change in the external magnetic field  $B_0$ , which is caused by temperature fluctuations in the laboratory. Although we tried to check the operating frequency regularly and correct any deviations with the screw shown above, this inconsistency of the operating frequency has effects on our measurement results that have yet to be discussed.

The computer measured the peak heights of the echo signals automatically. Among other things, the time  $\Delta T$  could be set, which is used before and after the peak to identify the frequency and

calculate the peak intensity. Brief experimentation showed that a decrease from the recommended value of 6 ms also resulted in a significant decrease in the measured intensity, so that we then also used 6 ms for all further measurements.

For measurements with short  $\tau$  it must also be considered that the signals of the  $90^\circ$  and  $180^\circ$  pulses overlap, which is another systematic source of error. Besides the uncertainty of the front values due to changing experimental conditions, it should also be noted that the rear values with large echo times may also contain errors. Finally, if echo times are too high, diffusion in the sample can help to ensure that the atoms are no longer all in phase again at the corresponding echo time, but reduce the intensity of the echo signal by independent migration and change of the magnetic field.

The results of the measurement for the Gd500 sample and the equivalent Gd600 sample are plotted with Python in Figure 7 and provided with an exponential fit according to equation 6. This way we

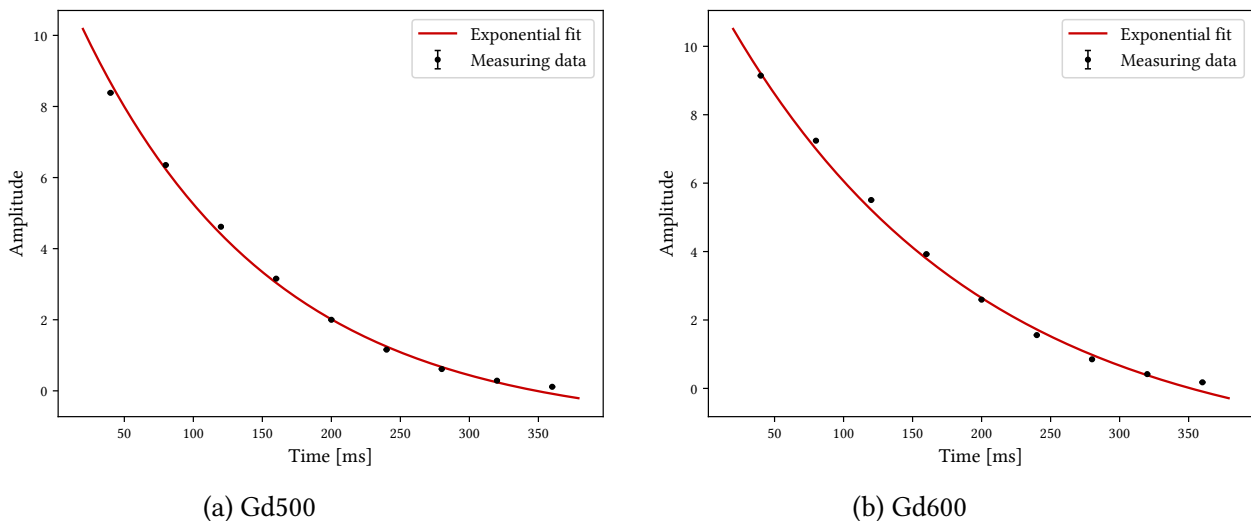


Figure 7: Results of the measurement for relaxation time  $T_2$  using spin-echo method

get the relaxation times

$$T_{2, \text{Gd500, spin-echo}} = (154.2 \pm 0.9) \text{ ms},$$

$$T_{2, \text{Gd600, spin-echo}} = (186.5 \pm 0.9) \text{ ms}$$

for our measurement.

### Spin-spin interaction $T_2$ using Carr-purcell method

The only difference between the Carr-purcell method and the previous spin-echo method is the recurring  $180^\circ$  pulse, so that echo signals appear again and again at intervals of  $2\tau$  and the exponential decrease in amplitude can already be seen at such a signal.

Because the values are recorded directly one after the other and possible inconsistencies in the magnetic field or other parts of the test setup do not have such a large influence, the results of the Carr-Purcell series of measurements appear more credible. After the Python fit we get the values

$$T_{2, \text{Gd500, Carr-purcell}} = (170.1 \pm 0.4) \text{ ms},$$

$$T_{2, \text{Gd600, Carr-purcell}} = (198.2 \pm 0.7) \text{ ms}$$

from figure 8.

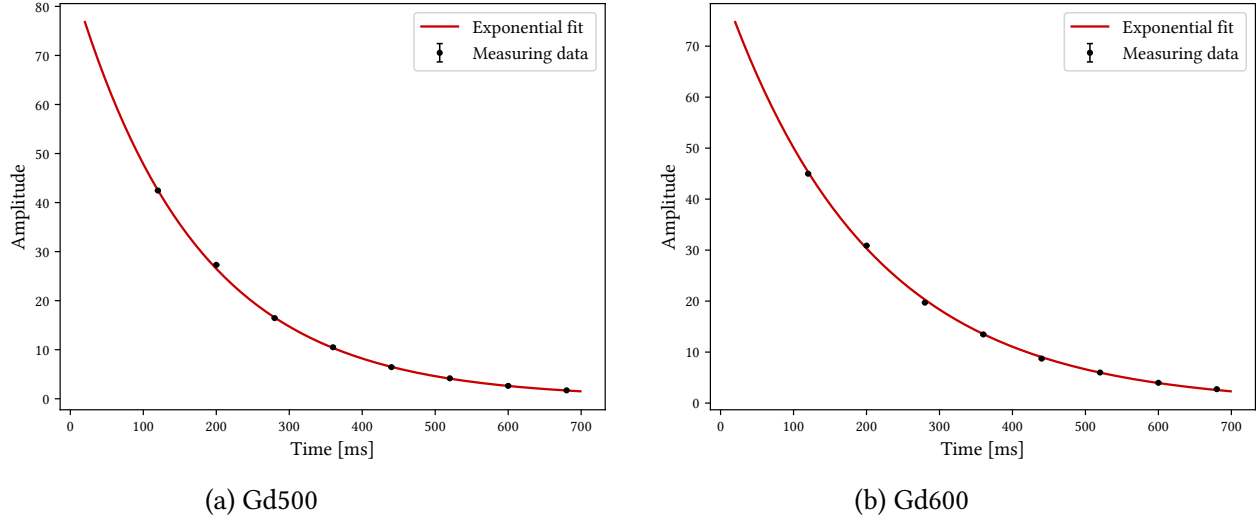


Figure 8: Results of the measurement for relaxation time  $T_2$  using Carr-purcell sequence.

### Spin-lattice interaction $T_1$

With the sequence of  $180^\circ$  and  $90^\circ$  pulses described in the basics after different long times and respective intensity measurement of the signal after this time, the increase of magnetization in the direction of the magnetic field can be measured.

The corresponding plots for the relaxation time of the spin-lattice interaction  $T_1$  for both gadolinium samples are shown in figure 9. With the help of Python, an exponential fit according to equation 5

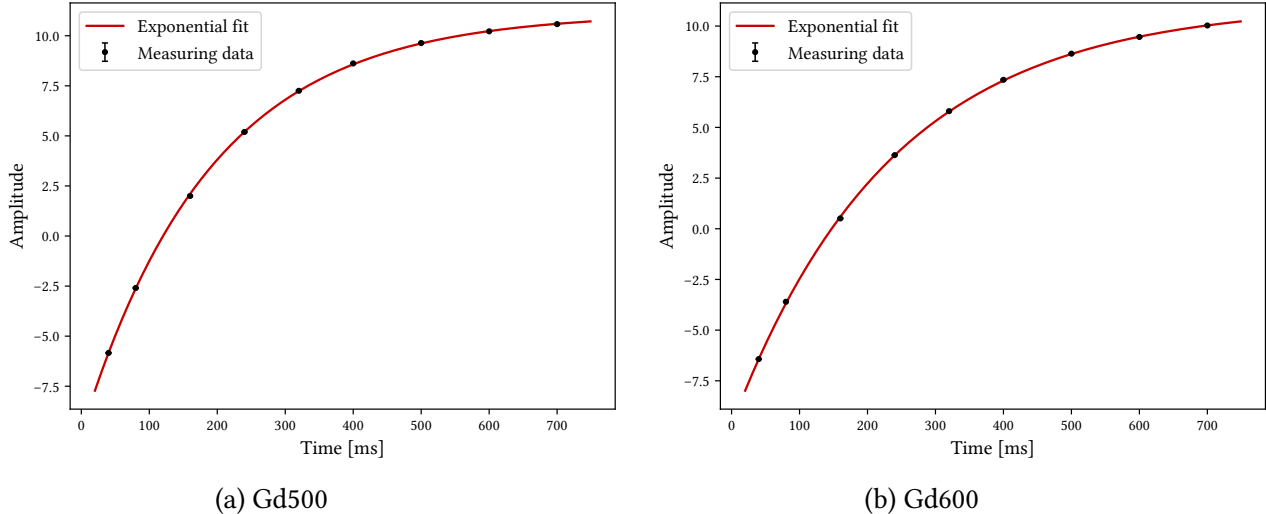


Figure 9: Results of the measurement for relaxation time  $T_1$ .

gives the values

$$T_{1, \text{Gd}500} = (190.0 \pm 0.6) \text{ ms},$$

$$T_{1, \text{Gd}600} = (234.3 \pm 0.5) \text{ ms}.$$

Table 1 summarizes all three measured relaxation time values for both samples. We see that all

Sample	$T_1$ [ms]	$T_{2, \text{spin-echo}}$ [ms]	$T_{2, \text{Carr-purcell}}$ [ms]
Gd500	$190.0 \pm 0.6$	$154.2 \pm 0.9$	$170.1 \pm 0.4$
Gd600	$234.3 \pm 0.5$	$186.5 \pm 0.9$	$198.2 \pm 0.7$

Table 1: Measured relaxation time.

relaxation times for the more diluted sample Gd-600 are longer than with Gd-500. This results directly from the higher water content or the associated higher density of hydrogen nuclei. Within the measurements of a sample we also see that the spin-echo method delivers shorter times than the Carr-purcell method. This is due to the longer recording time of the spin-echo method, in which the sample has time for diffusion and the magnetic field can change. The relaxation time  $T_2$  of spin-spin interaction is less than that of spin-lattice  $T_1$ , because the latter includes the energy release into the environment, while the former only takes into account the behavior within the molecules. In general, the theoretical prediction

$$T_1 \geq T_2$$

can be determined. In order to release energy into the environment, however, it requires a certain threshold value that is higher than that required to perform a spinflip in the molecules. Therefore, the time for the spin-lattice interaction is longer than for the spin-spin interaction.

## Chemical shift

In this part of the experiment we measured the Larmor frequencies of unknown substances with and without the reference substance TMS. This was done by measuring the resonance peaks of the Fourier transform of the registered signal. From the frequency shift measured in this way, the chemical shift can be calculated using equation 9.

Sample	Shift 1 [ppm]	Shift 2 [ppm]	Shift 3 [ppm]	Substance
A	$2.4 \pm 0.1$	$3.9 \pm 0.1$	$6.3 \pm 0.1$	fluoroacetone
B	$2.1 \pm 0.1$	$6.9 \pm 0.1$		p-xylol
C	$9.6 \pm 0.1$	$12.0 \pm 0.1$		acetic acid
D	$4.0 \pm 0.1$	$6.4 \pm 0.1$		fluoroacetonitril
E	$2.2 \pm 0.1$	$7.3 \pm 0.1$		tuluol

Table 2: Measured chemical shifts.

Experimentally, we had to give a pulse to the magnet every three seconds and continuously adjust the main magnetic field so that the working frequency is around  $\nu_w = 500$  Hz. Therefore, one wavelength had to be 2 ms long, which we could achieve via the screw on the magnet.

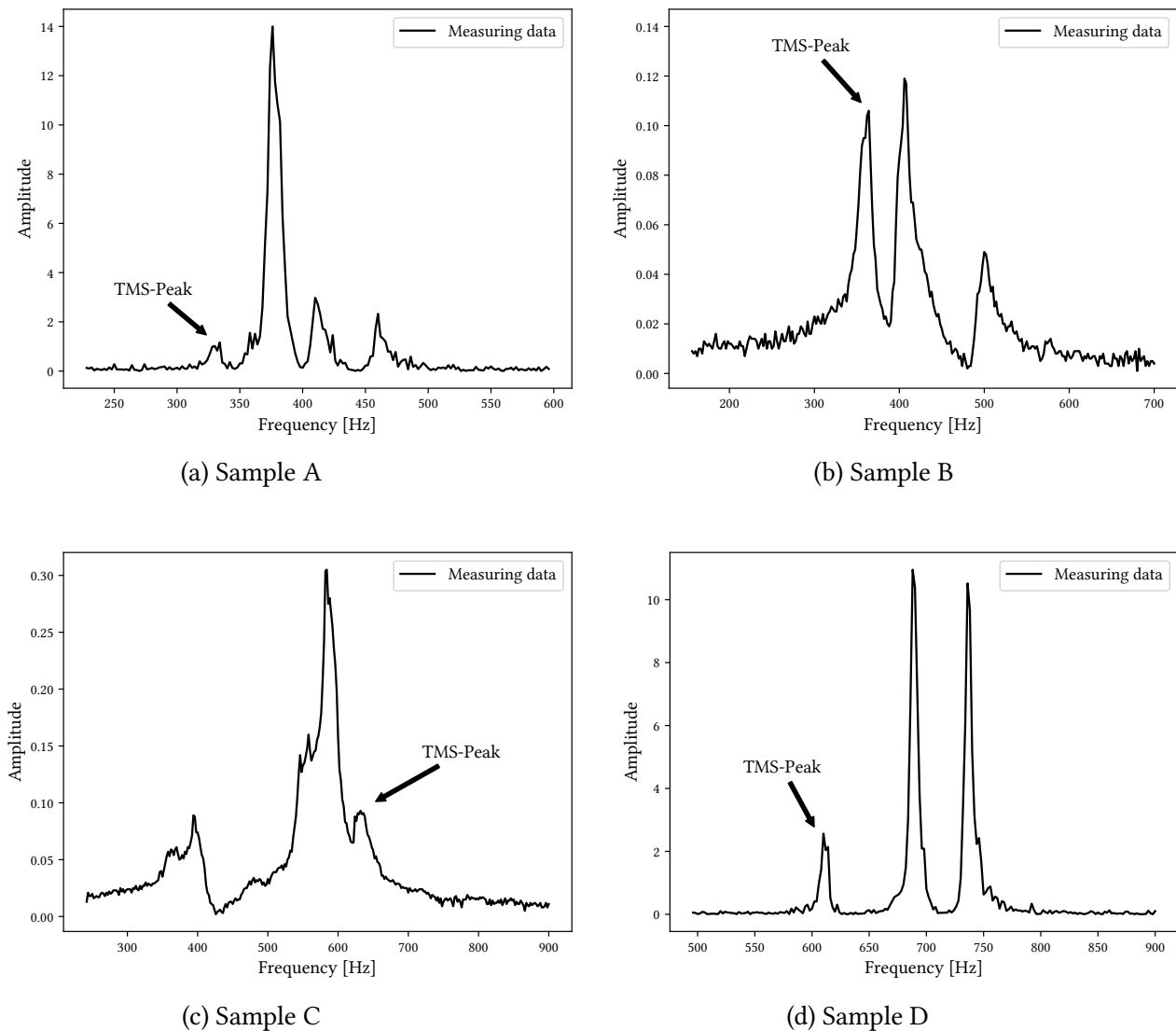


Figure 10: Fourier transform of the registered signal.

Table 2 lists the measured chemical shifts of the different samples and their assignment to the corresponding chemical elements. Due to missing samples A,D and E, the shifts could unfortunately only be taken over by leading test participants.

Now we knew that the elements toluol ( $\text{CH}_3 - \text{C}_6\text{H}_5$ ), p-xylol ( $\text{CH}_3 - \text{C}_6\text{H}_4 - \text{CH}_3$ ), acetic acid ( $\text{CH}_3 - \text{COOH}$ ), fluoroacetone ( $\text{FCH}_2 - \text{CO} - \text{CH}_3$ ) and fluoroacetonitrile ( $\text{FCH}_2 - \text{CN}$ ) were among the samples and could classify them according to the same principle with figure 3.

Sample C is the only one that has a shift above 10 ppm and therefore must have a COOH group, which only applies to acetic acid. The two shifts of samples B and E are in fact the same. The same functional groups, a carbon ring and one or two methyl groups for toluol and p-xylol, cause the same shifts. Because p-xylol contains twice the amount of methyl groups, this substance should show a higher ratio in the peak heights. Sample B shows exactly such a difference and is therefore p-xylol, while sample E is then toluol. Both fluoroacetone and fluoroacetonitrile have a fluoromethyl group and show two identical shifts. Nevertheless, the former has a third shift exactly the same size as

tuluol and p-xylol, which could be assigned to the simple methyl group. Therefore, sample A with the additional peak corresponds to fluoroacetone and sample D to fluoroacetonitril.

## Imaging techniques

The following part for the one and two dimensional imaging was performed with a Bruker NMR analyzer mq7. 5 and evaluated with software provided by Bruker.

### One dimensional imaging

First we examined the paintings of different heights of oil, as well as when Teflon layers are between the oil. Figure 11 shows very well the structural resolution of the NMR technology.

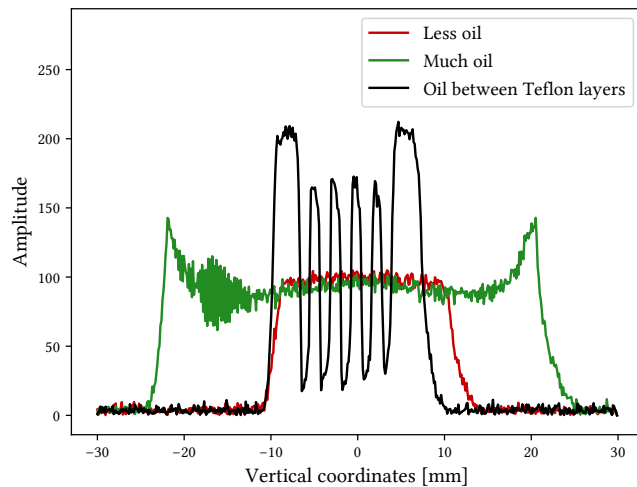


Figure 11: Various oil samples.

Since the analyzer used is calibrated for hydrogen, we expect signals proportional to the hydrogen density. For oil this corresponds to a square-wave signal, while Teflon consists of  $C_2F_4$  units and is therefore not excited.

At first glance you can see that the red curve only has a small but constantly wide peak for the small oil content. On the other hand, the green curve for the large amount of oil at both ends is increased again because the liquid does not “lie” perfectly in the test tube due to surface tension and edge effects on the test tube. In the black curve, the individual Teflon layers, which cannot be detected in the NMR and therefore have no amplitude, can be easily recognized again.

Furthermore, we filled a test tube up to about 2 cm with parrot sand and poured oil over it. Now we have made regular scans to investigate the seepage process (see fig. 12).

The question of whether this is diffusion can be answered with the help of Fick’s Law

$$\frac{\partial c}{\partial t} = D \frac{\partial^2 c}{\partial x^2} \quad (17)$$

where  $c$  is the concentration,  $t$  the time,  $D$  the diffusion coefficient and  $x$  the positive length.

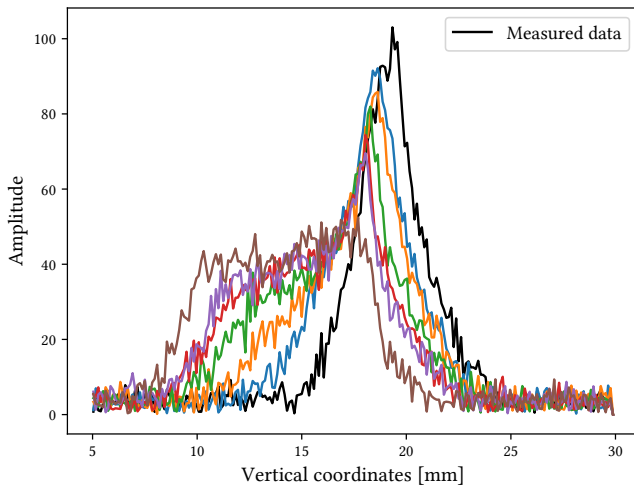


Figure 12: Seepage process of oil in sand (starts with black and ends with brown).

For this we consider a point in the sand at which there is no oil yet and therefore

$$\frac{\partial c}{\partial t} \geq 0$$

applies. Because  $D \geq 0$  also applies,

$$\frac{\partial^2 c}{\partial x^2} \geq 0$$

must also be fulfilled. But if we look at figure 12, we notice that this is not the case because the curves have several local extremes. Furthermore, a diffusion process must run in both negative and positive  $x$  directions, which is clearly not the case in our experiment. It is therefore not a diffusion process. This is also easy to understand, because besides Brown's molecular movement, gravity also acts as a driving force.

### Two dimensional imaging

In the last part of the experiment some organic substances were analysed in the test tube, this time two dimensional cross-sections were recorded. Areas in which water is contained produce a stronger signal. So, in figure 13a we will learn, that in an olive kernel there is also a liquid. The air pockets in the peanut are also clearly visible. But we have also noticed that the correct positioning of the sample plays an enormous role and thus quickly involves a great deal of time.

## 3. Critical Comment

This experiment was divided into work with a slightly older Bruker minispec p20 spectrometer and a Bruker NMR analyzer mq7.5. First of all, it can be generally said that the older device reacts very sensitively to temperature fluctuations, which is why we often had to readjust the working frequency. Nevertheless, the device was very descriptive and easily accessible from the outside, which makes it a good basis for nuclear magnetic resonance spectroscopy.

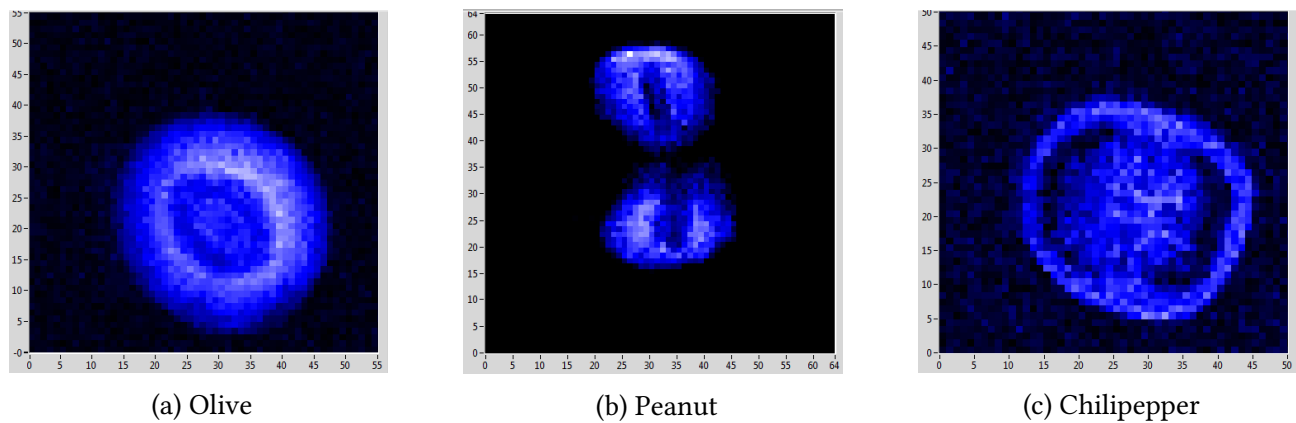


Figure 13: Two dimensional NMR imaging.

In the first part of the experiment we were able to measure the different relaxation times  $T_1$  and  $T_2$  of Gd500 and Gd600 with the device. We found the theoretically expected differences between the times of a sample as well as between the two samples. The times of Gd500 are smaller than those of Gd600 because gadolinium facilitates alignment in the magnetic field. The relaxation time  $T_2$  of spin-spin interaction is less than that of spin-lattice  $T_1$ , because the latter includes the energy release into the environment, while the former only takes into account the behavior within the molecules. In addition, the times of the spin echo method differ from those of the Carr-purcell method because the spin-echo method gives the sample a certain time to diffuse and the magnetic field can also change during this time.

In the second section we have determined the chemical displacement of various samples. This enabled us to assign functional groups and thus a chemical substance to each sample. The samples were rotated to compensate for inhomogeneities in the magnetic field. It is noticeable that the magnetic field is shielded differently by different groups, but the assignment by many overlaps is not so clear. This would certainly not be possible without a specification of the possible substances.

Then, using the new NMR analyzer, we used nuclear magnetic resonance spectroscopy for imaging, where the intensity of individual pixels is proportional to the water content. For example, we made one and two dimensional images of some organic and inorganic substances and examined their composition. The correct placement in the analyzer was essential, which quickly became a bit time-consuming. At the end, however, clear structures, such as the air pockets of a peanut, can be seen in the pictures.

Thus, the experiment was very good to gain insights into NMR, which is of course of great importance in medicine.

## References

- [1] R. Schicker. “Nuclear Magnetic Resonance F61/F62. Manual 2.0”. en. In: (Apr. 14, 2010). URL <https://www.physi.uni-heidelberg.de/Einrichtungen/FP/anleitungen/F61.pdf>.